Organic & Biomolecular Chemistry

RSC Publishing

PAPER

View Article Online
View Journal | View Issue

Cite this: *Org. Biomol. Chem.*, 2013, **11**, 2258

Cube-octameric silsesquioxane-mediated cargo peptide delivery into living cancer cells†

Sebastian Hörner,‡[a] Sebastian Fabritz,‡[a] Henry D. Herce,*[b,c] Olga Avrutina,[a] Christian Dietz,[d] Robert W. Stark,[d] M. Cristina Cardoso[c] and Harald Kolmar*[a]

Received 14th September 2012,
Accepted 6th December 2012

DOI: 10.1039/c2ob26808f

www.rsc.org/obc

Cube octameric silsesquioxanes (COSS) are among the smallest nanoparticles known to date with a diameter of only 0.7 nm. We describe a COSS-based delivery system which allows for the drug targeting in human cells. It comprises a siloxane core with seven pendant aminopropyl groups and a fluorescently labeled peptidic ligand attached to one cage corner *via* a reversible disulfide bond to ensure its intracellular release. Bimodal amplitude-modulated atomic force microscopy (AFM) experiments revealed the formation of dendritic COSS structures by a self-assembly of single particles on negatively charged surfaces. Nuclear targeting was demonstrated in HeLa cells by selective binding of released p21$^{Cip1/Waf1}$-derived cargo peptide to PCNA, a protein involved in DNA replication and repair.

Introduction

Nanomaterials and nanoparticles with tailor-made functionalities attract growing interest in the fields of gene therapy,[1] DNA protection,[2] or cancer targeting.[1–3] In molecular oncology, they enable cell penetration acting as modules for drug delivery into tumor cells. *In vivo*, the enhanced permeability and retention effect[4,5] as well as the leaky vasculature of cancer cells result in a passive targeting of nanoparticle-delivered drugs.[6,7] Size, shape, surface charge, and the functional groups of a nanoparticle control its interaction with biological systems.[8,9] Thus, the functionality but also the toxicity of nanoparticle-based delivery units strongly depends on their design.[10,11] Therefore, it is essential to ensure a balance between the desired biological function and cytotoxicity due to *e.g.* reactive oxygen species[10] or vasculature obstruction resulting in organ-associated toxicity.[11] Considering these requirements, a wide range of cell membrane-permeable nanoparticles has been developed, among them core–shell fluorescent,[12] mesoporous dye-doped,[13,14] TAT[15]-peptide-conjugated[16,17] silica nanoparticles (SNP) and nanovalves.[18–20]

Cube-octameric silsesquioxanes (COSS)[21] can be considered as special members of the SNP family. They are highly symmetric molecules of pico dimension comprising a 500 pm silica core that is decorated with organic ligands.[22] COSS with pendant azide,[23–25] aminooxy,[22] vinyl,[26] thiol[27] or amine[28] functionalities allow for the presentation of biomolecules such as carbohydrates,[19,25,26,29] peptides,[22,23] and miniproteins[22] using the respective conjugation chemistry. Thus, up to eight ligands can be covalently attached to the silsesquioxane scaffold (Scheme 1a).

Comparing the size of COSS nanoparticles with the dimensions of other nanomaterials (*e.g.* silica and gold nanoparticles or biocompatible polymers), it is evident that a COSS cage is significantly smaller. This feature could be advantageous *e.g.* for enhanced vascular distribution or deeper tissue penetration. The cubic structure of the inorganic core allows for extremely dense presentation of functional ligands within an exactly defined architecture. Hydrolytic degradation of the inorganic COSS core into well-known primary silsesquioxanes at physiological pH[19,30] makes these molecules biodegradable scaffolds with potentially reduced risk of renal accumulation. However, the aspect of biodistribution and biostability of modified cube-octameric silsesquioxanes is largely unexplored and requires further systematic studies.

Among others, COSS carrying either lysine dendrimers[31] or poly(2-dimethylamino)ethyl methacrylate chains,[32] respectively, have been reported as DNA delivery systems into cells.

[a]*Clemens-Schöpf Institute of Organic Chemistry and Biochemistry, Technische Universität Darmstadt, Petersenstr. 22, 64287 Darmstadt, Germany. E-mail: Kolmar@Biochemie-TUD.de*
[b]*Department of Physics, Rensselaer Polytechnic Institute, Center for Biotechnology and Interdisciplinary Studies, Building 3237, 110 8th Street, Troy, NY 12180, USA. E-mail: hdherce@gmail.com*
[c]*Fachbereich Biologie, Technische Universität Darmstadt, Schnittspahnstraße 10, 64287 Darmstadt, Germany*
[d]*Center of Smart Interfaces, Technische Universität Darmstadt, Petersenstr. 32, 64287 Darmstadt, Germany*

†Electronic supplementary information (ESI) available: RP-HPLC spectra of **2**, **2a**, **3**, **4**, **5**, **5a**; ESI-MS data of **2**, **3**, **5**, **5a**, **5b**; HR-MS data of **2a**, **4**; IR spectrum of **4**. See DOI: 10.1039/c2ob26808f

‡These authors contributed equally to this work.

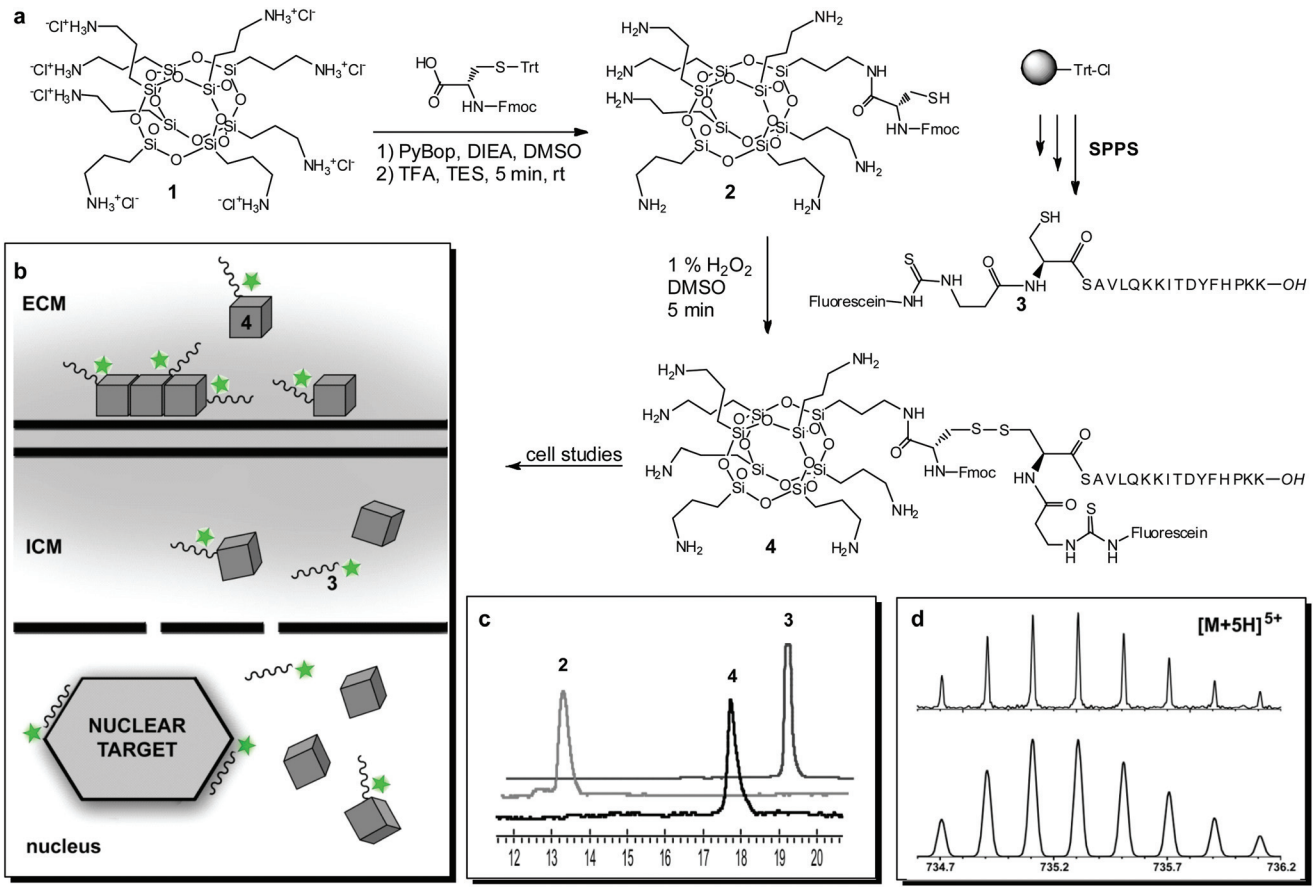

Scheme 1 (a) Synthesis of a biodegradable COSS–peptide conjugate **4**. The sequence of a p21$^{Cip1/Waf1}$-based peptide cargo is shown using a one-letter code; SPPS – solid phase peptide synthesis; (b) studies in HeLa cells using **4** are depicted as cartoon. **4** was applied to the extracellular medium (ECM) and penetrated the cell outer membrane. In the intracellular medium (ICM) the nanoparticle was accumulated in the nucleoli allowing for the targeting of the nucleus abundant protein PCNA; (c) HPLC traces (220 nm, 25% → 50% aq. CH_3CN in 20 min) recorded upon synthesis of **4**; (d) high-resolution mass spectrometric isotopic pattern; calc. for **4** $C_{158}H_{246}N_{35}O_{45}S_3Si_8$ (5+): 734.7065, meas. 734.7077.

Nanodots composed of a COSS cage surrounded by cationic-conjugated electrolyte arms could be targeted to the cell nucleus upon folic acid functionalization.[33]

In addition to nanoparticles that contain large and branched side chains extending from the inorganic silica core, cell-penetrating COSS derivatives have been described that bear relatively short arms, *i.e.* an isobutyl[34] or aminopropyl side chain.[35] Interestingly, McCusker *et al.* have demonstrated that fluorescently labeled water-soluble ammonium-functionalized COSS penetrated the outer membrane of Cos-1 cells[36] while exhibiting very low toxicity.[35] Based on these findings, the general applicability of octaamino COSS as a very small nanoparticle drug carrier was postulated, albeit an experimental proof is still missing.[35]

Herein, we investigated the applicability of octaamino COSS nanoparticles as a delivery system for targeting a peptidic cargo molecule to the nucleus of human HeLa[37] cancer cells.

As a model peptide for cargo delivery a 16-mer peptide SAVLQKKITDYFHPKK[38] was chosen that is known to bind an abundant nuclear protein, the proliferating cell nuclear antigen (PCNA).[39] PCNA is an essential component of the DNA replication and repair machinery and plays a fundamental role in cell proliferation and genome stability.[38–40] Tumor theranostic-related research in this field is concentrated on the development of a cancer biomarker based on the immunostaining of cancer-associated PCNA isoforms[41] and the inhibition of DNA replication *via* binding of peptidic ligands to PCNA.[38] The peptide mentioned above is derived from protein p21$^{Cip1/Waf1}$ that is known to bind PCNA,[42] thus playing a crucial role in regulating its activity.[43] An oligopeptide comprising the PCNA binding sequence of p21$^{Cip1/Waf1}$ was delivered into C2C12[44] mouse myoblast cells *via* TAT-mediated transduction. It caused cell cycle arrest indicating direct interference with protein–protein interaction that is crucial for DNA replication and repair.[45]

Results and discussion

For initial experiments, a single corner of the octaamino COSS particle was modified with a C-terminally fluorescein-labeled Cys-βAla dipeptide (Fig. 1a) and human HeLa cells were

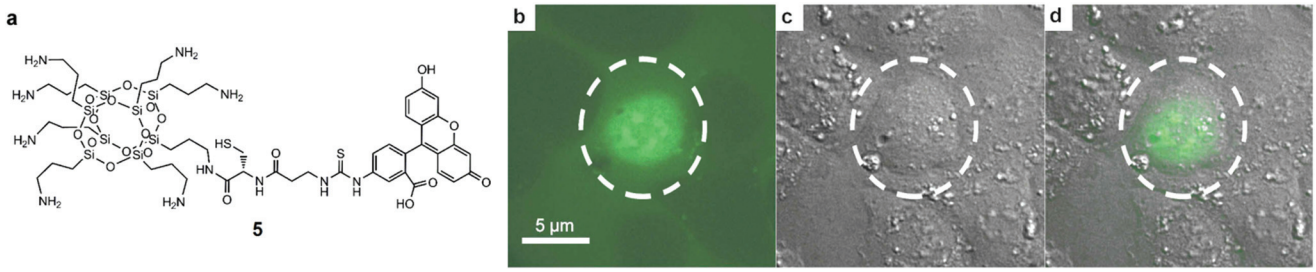

Fig. 1 Cellular uptake of fluorescein-labeled octaamino COSS **5** (a). The nanoparticle was added to the extracellular medium (final concentration of 20 μM) and after 30 min incubation the cells were washed with phosphate buffered saline and imaged. (b) Fluorescence image, (c) contrast image, (d) overlay. The location of the nucleus is indicated by a dotted circle.

incubated with the resulting conjugate (20 μM) for 30 min. Confocal microscopy studies revealed the distinct accumulation of silsesquioxanes in the multiple nucleoli of HeLa cells and also, to a lower extent, throughout the nucleoplasm and cytoplasm (Fig. 1b–d). This is in accordance with previous findings for nuclear localization of gold nanoparticles having the size of 2400 pm.[46] Due to their small size, the transit of COSS derivatives (700–800 pm) through the nuclear pore complex with an internal diameter of about 30 to 50 nm[47–49] might be achieved by passive diffusion. The observed accumulation in the nucleoli could be enhanced *via* electrostatic interactions of positively charged SNPs and phosphate-rich RNA. Providing clear evidence that amino silsesquioxanes are accumulated in the nucleoli of HeLa cells, our data differ from the reported lack of nuclear uptake of octaammonium COSS in a Cos-1 cell assay.[35] This discrepancy might be caused by the distinct nature of the used cell lines. Indeed, Cos-1 is a monkey-derived immortalized fibroblast-like cell line,[50] whereas HeLa is a human-derived cervical cancer cell line.[51]

After having confirmed intracellular and nuclear accumulation of COSS, the p21-derived peptide was covalently attached to a single-corner cysteine-modified octaamino COSS through a reversible disulfide bond (Scheme 1). Being sensitive to reducing conditions inside living cells,[52] the disulfide bond is well known to dissociate after cell penetration thereby releasing the attached cargo molecule from the carrier.[52] An additional fluorescein moiety was introduced into this hybrid construct allowing for live-cell confocal[53] microscopy studies.

As cell penetration, toxicity and nuclear targeting depend on the size and shape of the applied SNPs, bimodal amplitude-modulated atomic force microscopy (AFM)[54–56] was used to further characterize particle **4**. Depending on the particle concentration in the initial solution, we observed two types of particle arrangements on a mica surface: globular particle assembly (Fig. 2a and 2b) and dendritic structures (Fig. 2c–2h). Fig. 2a shows an amplitude-modulated AFM topography image of solitary and assembled COSS particle **4**. The cross-section analysis (Fig. 2a and 2b) reveals three distinctive heights: ≈700 pm, 1400 pm and 2100 pm, suggesting a single particle size of 700 pm and multiples of it. At higher

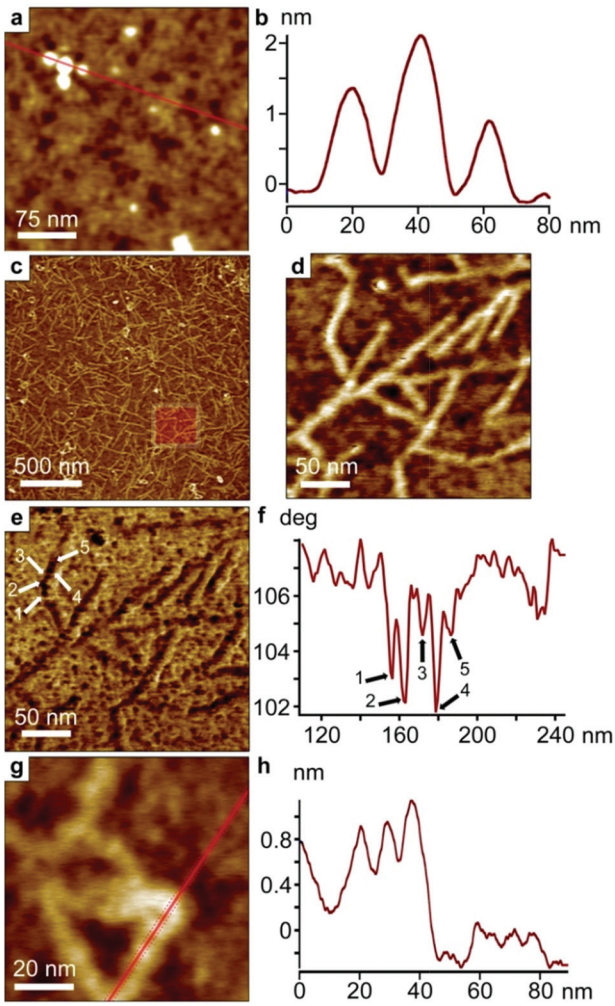

Fig. 2 (a) AFM topography image of singular and globular COSS–peptide particles **4**; (b) three particle profile from a section along the red line in (a); (c) and (d) AFM topography image of self-assembled SNP **4**; (e) second eigenmode phase image corresponding to (d). The image allows for the detection of single particles within the dendritic structure; (g) high-resolution frequency modulated AFM image of self-assembled **4**; (h) corresponding particle profile.

concentrations dendritic structures of **4** can be seen in the topographical image of Fig. 2c. Here, bimodal AFM was applied to enhance the lateral resolution of the phase images,

giving the height of the ordered structures as ≈700–800 pm (Fig. 2d). The corresponding second eigenmode phase image (Fig. 2e) clearly depicts the arrangement of single particles within one chain. Particles appear as dark dots (phase shift ≈102–104°), whereas the mica substrate shows a phase shift of ≈108°. In the profile (Fig. 2f) these particles are well separated. This leads to the conclusion that the dendritic structures are formed by a self-assembly of single SNPs **4** arranged next to each other. Frequency-modulated AFM topography images (Fig. 2g and 2h) corroborated these findings. Because this technique is extremely sensitive to topographical variations, even single particles were distinguished in the height profile. A similar self-assembly of silsesquioxane monomers may occur on a cell surface as well. However, the issue remains open whether the monomeric octaammonium COSS or self-assembled polymers are preferably involved in uptake and cell penetration. We suppose that the difference between heptalysine which lacks membrane permeability[57] and cell-penetrating octaaminosilsesquioxanes could be explained by the higher charge density within COSS and its shape-dependent self-assembly.[58–60] It might allow these cube-octameric SNPs to act as polycationic polymers (*e.g.* polylysine or polyethyleneimine) which are known to penetrate cell membranes.[61] It will be interesting to see, whether variation of the spatial arrangement and nature of the cationic groups have an influence on cellular uptake of COSS and on the uptake mechanism, which has to be elucidated yet.

It remained to be investigated, whether the COSS-bound cargo peptide displays biological activity which, in this experimental setting, is binding to PCNA. To address this question, co-localization experiments were performed involving fluorescein-labeled peptide **3** and PCNA, which was expressed as a fusion protein with red fluorescent protein (mRFP)[62] *via* transient transfection of HeLa cells with a mammalian expression plasmid coding for mRFP-tagged PCNA. PCNA is known to accumulate at sites of DNA damage that can be induced locally *via* UV microbeam irradiation (Fig. 3 and S18†).[63] To this end, a spot in a nucleus of a HeLa cell treated with a 20 μM solution of **4** was micro-irradiated for 1.2 seconds. Within 20 min RFP-labeled PCNA could be visualized at the site of DNA damage.[63] Co-localization of the fluorescent signal of **3** provided evidence of its accumulation at the DNA repair site (Fig. 3b and 3d). This clearly demonstrates that a significant portion of the cargo is able to freely address a target site in a HeLa cell nucleus.

Release of a peptide from a disulfide-bound cell-penetrating peptide carrier in the reducing milieu of a cell is a process that occurs relatively fast.[52,64] This is corroborated by our finding that the fluorescently labeled nanoparticle **5** is predominantly found in the nucleus while the COSS-bound labeled peptide **3** is also detected in the cytoplasm 30 min after incubation (Fig. S18†), which indicates a release from the carrier. Hence, it is most likely the liberated peptide **3** that interacts with PCNA rather than the COSS–peptide complex **4**.

For drug delivery, interactions of the carrier with a biological system that may eventually result in cell toxic effects are not desired, except those important for directed transit. Indeed, non-porous SNPs presenting primary amines at their surface have been reported to exhibit low toxicity[11,35] and degrade[65,66] under physiological conditions.[19,30] Here we corroborate these findings for amino-functionalized COSS with a cell viability assay based on the enzymatic reduction of the tetrazole XTT[67] using a single-corner cysteine-modified octaamino COSS. Within 12 hours, an SNP solution with a concentration of ~70 μM was needed to kill half of the cell population. Considering the reported lack of toxicity for non-functionalized octaaminopropyl COSS,[19,35] concentration-dependent reduced cell viability may be caused by the presence of the Fmoc-L-cysteine moiety attached to one of the cage corners rather than the COSS itself. Nevertheless, the concentration of SNP, which was used for the targeted delivery into the cell, is significantly lower than the concentration at which toxicity was observed (Fig. 4).

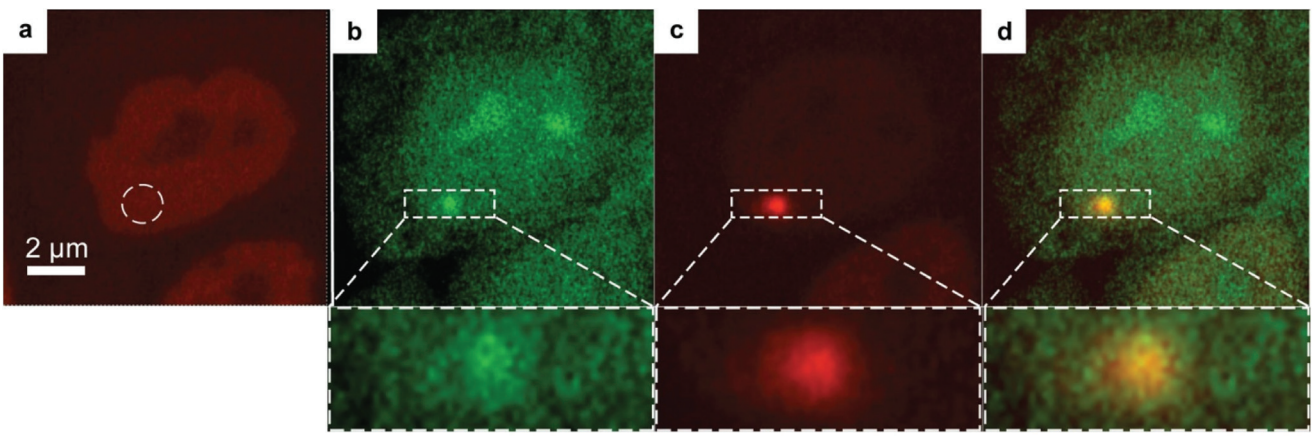

Fig. 3 (a) Micro-irradiation at the circle position (1.2 s) of a HeLa cell using a 405 nm laser; (b)–(d) co-localization of **3** and PCNA after cell incubation with **4** for 30 minutes at 37 °C. PCNA is recruited to repair micro-irradiated damaged DNA; (b) fluorescence signal of **3** (green); (c) fluorescence signal of red fluorescent protein labeled PCNA; (d) overlay of (b) and (c).

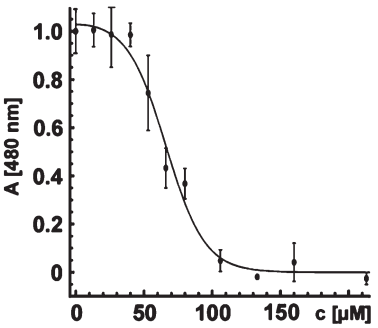

Fig. 4 The cell viability test using a single-corner cysteine-modified octaamino COSS. At a nanoparticle concentration of ~70 μM half of the observed cell population died, whereas a concentration of ~120 μM killed all cells within 12 hours.

Conclusion

In conclusion, a COSS derivative was synthesized which comprised a siloxane core with seven pendant aminopropyl groups and a peptidic ligand attached to one cage corner through a reversible disulfide bond. This architecture allowed for the penetration of human cells and peptide accumulation in the cell nucleus. Nuclear drug targeting was demonstrated in HeLa cells using a fluorescently labeled p21$^{Cip1/Waf1}$-derived peptide as a COSS cargo, which selectively bound PCNA, a protein involved in DNA replication and repair. In perspective, it might be interesting to study the octaamino COSS uptake mechanism in further detail by AFM and fluorescence microscopy studies on artificial lipid membranes[68,69] and cells. Finally, it remains to be elucidated whether silsesquioxane-based cargo delivery allows for the targeting of other proteins both in the nucleus and cytoplasm.

Experimental

HPLC analysis and purification

For RP-HPLC analysis a Varian 940-30 LC equipped with a Phenomenex Luna C_{18} column (5u, 100 A, 250 × 4.60 mm, 5 μm) was used at a flow rate of 1 mL min^{-1}. For isolation of products by RP-HPLC a C_{18} column (250 × 20 mm; S-4 μm, 8 nm) was employed at a flow rate of 18 mL min^{-1}. Eluent A: 0.1% aq. trifluoroacetic acid (TFA), eluent B: 90% aq. MeCN in 0.1% aq. TFA. 5 min of isocratic flow (starting concentration of eluent B) was followed by 20 min of gradient flow.

Compound 1

Synthesis of octaammonium COSS. According to a modified procedure reported by Feher and Wyndham,[70] 25 mL (23.7 g, 0.107 mol) 3-(triethoxysilyl)-1-propanamine were dissolved in 600 mL methanol. 34.0 mL concentrated hydrochloric acid (HCl) were added and the reaction mixture was stirred at room temperature. After 4 weeks, a white precipitate was formed. The suspension was stirred for additional two weeks. The precipitate was separated by filtration, washed 2 times with ice-cold acetone and dried in a desiccator. 3.08 g of white solid were obtained (23.0%).

^{1}H NMR [300.0 MHz, DMSO-d$_6$, room temp.] δ 8.25 (s, NH_3^+, 24 H), 2.79 (t, $CH_2NH_3^+$, 16 H), 1.74 (m, $SiCH_2CH_2$, 16 H), 0.74 (t, $SiCH_2$, 16 H). ^{13}C NMR [75.4 MHz, DMSO-d$_6$, room temp.] δ 40.95 (s, $CH_2NH_3^+$), 20.55 (s, $SiCH_2CH_2$), 8.37 (s, $SiCH_2$). ^{29}Si NMR [59.6 MHz, DMSO-d$_6$, room temp.] δ −66.41. ESI-MS calc. for **1** $C_{24}H_{64}N_8O_{12}Si_8$ *m*/*z*: 881.5, meas. 881.5 $[M + H]^+$; calc. 441.8, meas. 441.8 $[M + 2H]^{2+}$.

Compound 2

Synthesis of Fmoc-(S-trityl)-L-cysteine heptaammonium-COSS (2a). To a mixture of 10.5 mg (0.018 mmol, 2.1 equiv.) of Fmoc-(S-trityl)-L-cysteine and 8.9 μL dry DIEA (6.6 mg, 0.051 mmol, 6.0 equiv.) in 1 mL dry dimethylsulfoxide (DMSO), 8.9 mg (0.017 mmol, 2.0 equiv.) of (benzotriazol-1-yloxy)tripyrrolidinophosphonium hexafluorophosphate (PyBOP) in 1 mL dry DMSO were added dropwise. The mixture was incubated for 10 min at room temperature and afterwards diluted with dry DMSO to a volume of 12 mL.

10 mg (0.0085 mmol, 1.0 equiv.) of **1** were dissolved in 0.5 mL dry DMSO and vigorously stirred. The previously described mixture was added slowly using a peristaltic pump (flow: 0.05 mL min^{-1}). After complete addition, the mixture was stirred for 1 hour at room temperature. The solvent was removed by lyophilization. The resulting oil was suspended in 5 mL of 0.01 M HCl and again lyophilized. The white powder was suspended in dry acetonitrile and the insoluble part was washed two times with dry acetonitrile. The precipitate was dried *in vacuo* and purified by semipreparative RP-HPLC. After lyophilization, 3.0 mg of white solid were obtained (24.4%).

RP-HPLC, 10 → 80% B, t_R = 20.1 min. HR-MS calc. for **2a** $C_{24}H_{79}N_9O_{15}SSi_8$ *m*/*z*: 724.7406, meas. 724.7409 $[M + 2H]^{2+}$ (see Fig. S2 and S3†).

Deprotection of Fmoc-(S-trityl)-L-cysteine heptaammonium-COSS. 3.0 mg of Fmoc-(S-trityl)-L-cysteine heptaammonium-COSS were dissolved in 500 μL TFA and 5 μL (1 vol%) triethylsilane (TES) were added. The mixture was shaken for 30 min at room temperature and the solvent was removed *in vacuo*. The colorless residue was dissolved in deionized water and the solvent was removed by lyophilization. The product was used without further purification.

RP-HPLC 10 → 80% B, t_R = 16.7 min. ESI-MS calc. for **2** $C_{42}H_{79}N_9O_{15}SSi_8$ *m*/*z*: 1206.9, meas. 1206.6 ($[M + H]^+$); calc. 604.4, meas. 604.4 $[M + 2H]^{2+}$; calc. 403.3, meas. 403.3 $[M + 3H]^{3+}$ (see Fig. S4†).

Compound 3

Synthesis of fluorescein-labeled PCNA binding peptide. Microwave-assisted Fmoc-SPPS of PCNA binding peptide **3** was performed on 2-chlorotrityl resin (*Iris Biotech* GmbH) (0.25 mmol) using a CEM *Liberty*® peptide synthesizer equipped with a CEM *Discover*® SPS microwave (CEM GmbH). All amino acids were attached by triple coupling using 4.0 equiv. of the amino acid, 3.9 equiv. of *O*-(benzotriazol-1-yl)-*N*,*N*,*N*′,*N*′-tetramethyluroniumhexafluorophosphate (HBTU)

(*Iris Biotech* GmbH), and 8 equiv. of base (DIEA for all amino acids except cysteine; for coupling of Fmoc-(S-trityl)-L-cysteine, collidine (*Sigma-Aldrich*) was used) in *N*,*N*′-dimethylformamide (DMF). Triple coupling (30 W, 50 °C, 15 min) and double deprotection (30 W, 50 °C, 5 min) of the amino acids were performed upon microwave assistance. Fluorescein isothiocyanate (FITC) was coupled manually to the resin-bound peptide. 194.7 mg (0.50 mmol, 2 equiv.) FITC and 87.2 μL (64.7 mg, 4.0 equiv.) dry DIEA were dissolved in 5 mL dry DMF and the solution was added to the resin-bound peptide. The mixture was heated 3 times in a microwave (30 W, 50 °C, 30 min). Afterwards, the mixture was shaken at room temperature overnight. The peptide was cleaved from the resin and purified by semi-preparative RP-HPLC yielding 37.0 mg of a yellow solid after lyophilization (6.0%).

RP-HPLC, 30 → 40% B, t_R = 20.0 min. ESI-MS calc. for **3** $C_{116}H_{164}N_{26}O_{30}S_2$ *m*/*z*: 1234.4, meas. 1234.5 $[M + 2H]^{2+}$; calc. 823.3, meas. 823.3 $[M + 3H]^{3+}$; calc. 617.7, meas. 617.8 $[M + 4H]^{4+}$; calc. 494.4, meas. 494.5 $[M + 5H]^{5+}$ (see Fig. S6 and S7†).

Compound 4

Coupling of PCNA binding peptide to 2. 1.6 mg (0.0014 mmol, 1 equiv.) of **2** and 10.0 mg (0.0040 mmol, 3 equiv.) of compound **3** were dissolved in 200 μL dry DMSO. 10 μL 30 vol% aqueous hydrogen peroxide were mixed with 100 μL dry DMSO and quickly added to the mixture resulting in a 1 vol% solution of hydrogen peroxide. The probe was vigorously shaken for 5 min at room temperature. Immediately, 1 mL of deionized water was added and the probe was frozen in liquid nitrogen. The solvent was removed by lyophilization and the resulting solid was purified by RP-HPLC. After lyophilization, 1.4 mg of yellow solid was obtained (23.0%).

RP-HPLC, 27 → 40% B, t_R = 17.8 min. HR-MS calc. for **4** $C_{158}H_{241}N_{35}O_{45}S_3Si_8$ *m*/*z*: 734.7065, meas. 734.7077 $[M + 5H]^{5+}$. IR: 2912, 1629, 1530, 1104 cm^{-1} (see Fig. S9, S10, and S11†).

Compound 5

Synthesis of Cys-(S-trityl)-β-Ala-fluorescein (5a). Microwave-assisted Fmoc-SPPS of dipeptide Cys-(S-trityl)-β-alanine-fluorescein was performed at 0.10 mmol scale on 2-chlorotrityl resin (*Iris Biotech* GmbH). 58.6 mg (0.10 mmol, 1 equiv.) Fmoc-(S-trityl)-L-cysteine (*IRIS Biotech* GmbH) and 52.9 μL (48.5 mg, 0.40 mmol, 4 equiv.) collidine (*Sigma-Aldrich*) were dissolved in 3 mL dry DCM and the solution was added to the resin and shaken for 2 hours at room temperature. The Fmoc protecting group was removed by double deprotection using a CEM *Discover*® SPS microwave (CEM GmbH) (30 W, 50 °C, 5 min). Coupling of Fmoc-β-alanine (*IRIS Biotech* GmbH) was performed as a triple coupling using 4.0 equiv. Fmoc-β-alanine, 3.9 equiv. HBTU, and 8 equiv. DIEA in DMF in a microwave (30 W, 50 °C, 15 min). 78.0 mg (0.20 mmol, 2 equiv.) FITC and 69.5 μL (51.6 mg, 4.0 equiv.) dry DIEA were dissolved in 2 mL dry DMF and the solution was added to the resin-bound dipeptide. The mixture was heated 3 times (30 W, 50 °C, 30 min) in a microwave. Afterwards, the mixture was shaken at room temperature overnight. For cleavage of the peptide, 5.0 mL of a mixture of acetic acid, methanol, and DCM (5 : 1 : 4, v : v : v) were added. The mixture was shaken for 3 hours at room temperature. Afterwards the solution was added dropwise to 45.0 mL of ice-cold methyl *tert*-butyl ether (MTBE). The yellow precipitate was purified by semi-preparative RP-HPLC. Lyophilization gave 52.4 mg of a yellow solid (63.6%).

RP-HPLC, 10 → 100% B, t_R = 23.7 min. ESI-MS calculated for **5a** $C_{46}H_{37}N_3O_8S_2$ *m*/*z*: 823.9, meas. 824.4 $[M + H]^+$ (see Fig. S13 and S14†).

Synthesis of Cys-(S-trityl)-β-Ala-fluorescein heptaammonium-COSS (5b). 7.7 mg (0.0094 mmol, 1.1 equiv.) of the dipeptide Cys-(S-trityl)-β-alanine-fluorescein, 1.6 mg (0.0085 mmol, 1 equiv.) of 1-ethyl-3-(3-dimethylaminopropyl)-carbodiimide (DIC) and 6 μL (4.4 mg, 0.034 mmol, 4 equiv.) of dry DIEA were dissolved in 500 μL dry DMSO. The mixture was shaken for 10 min at room temperature and 10.0 mg (0.0085 mmol, 1 equiv.) of compound **1** dissolved in 500 μL dry DMSO were added. The mixture was shaken for 4 days in the dark and poured into 12 mL of dry acetonitrile. The yellow precipitate was washed two times with dry acetonitrile. It was purified by semi-preparative RP-HPLC. After lyophilization, 4.4 mg of yellow solid were obtained (27.8%).

RP-HPLC, 10 → 100% B, t_R = 16.0 min. ESI-MS calc. for **5b** $C_{70}H_{99}N_{11}O_{19}S_2Si_8$ *m*/*z*: 844.7, meas. 844.8 $[M + 2H]^{2+}$; calc. 563.5, meas. 563.5 $[M + 3H]^{3+}$; calc. 422.9, meas. 422.9 $[M + 4H]^{4+}$ (see Fig. S16†).

Deprotection of Cys-(S-trityl)-β-Ala-fluorescein heptaammonium-COSS. 4.4 mg of Cys-(S-trityl)-β-Ala-fluorescein heptaammonium-COSS were dissolved in 0.5 mL TFA and 5 μL (1 vol%) of triethylsilane (TES) (*Alfa Aesar*) were added. The mixture was shaken for 30 min at room temperature and the solvent was removed *in vacuo*. The yellow residue was purified by semi-preparative RP-HPLC. After lyophilization, 2.0 mg of yellow solid were obtained (53.0%).

RP-HPLC, 10 → 100% B, t_R = 14.0 min. ESI-MS calc. for **5** $C_{51}H_{85}N_{11}O_{19}S_2Si_8$ *m*/*z*: 723.6, meas. 723.5 $[M + 2H]^{2+}$; calc. 482.7, meas. 482.7 $[M + 3H]^{3+}$ (see Fig. S17†).

Atomic force microscopy. We conducted atomic force microscopy experiments on air using a Cypher AFM (*Asylum Research*, Santa Barbara, CA, USA) and PPP-ZEIHR cantilevers (*NanoandMore* GmbH, Wetzlar, Germany). Bimodal AFM was done with the first two eigenfrequencies at $f_1 \approx 130$ kHz and $f_2 \approx 820$ kHz. The free oscillation amplitudes were driven to $A_{01} \approx 10$ nm and $A_{02} \approx 1$ nm, respectively. A high amplitude setpoint ratio $A_{sp}/A_{01} \approx 0.9$ was chosen ensuring that the AFM is operated in the net attractive regime where mechanical repulsion is minimized and hence, the impact of the tip on the sample is small.

High-resolution frequency-modulated AFM measurements were accomplished using the same type of cantilever. For tracking the frequency, an external phase-locked-loop PLLPro2 (*RHK Technology*, Troy, MI, USA) was integrated into the feedback loop of the AFM. We kept the cantilever vibrating at a constant frequency shift of $\Delta f = 50$ Hz with respect to the free oscillation and the amplitude was maintained at $A_0 \approx 10$ nm. Images (512 × 512 pixel) were obtained with a scan speed of 500 nm s^{-1}.

Cell culture and fluorescein-labeled COSS cellular uptake. HeLa cells were seeded at 80% confluency into 24-well microscope observation chambers (*Ibidi*, Munich, Germany) and the growth medium (Dulbecco's modified Eagle medium; PAA) DMEM supplemented with 10% fetal calf serum (*Life Technologies*) and gentamycin was exchanged against the COSS solutions. COSS were diluted to 20 μM final concentration in 400 μL DMEM and incubated with the HeLa cells for 30 min at 37 °C prior to imaging.

Cell viability assay. HeLa cells were seeded at 70% confluency in 24-well plates and incubated for one hour at different COSS concentrations. The media were subsequently exchanged for DMEM without COSS and the cells were incubated for 12 hours. Then the media were exchanged with serum-free DMEM and 0.3 mg mL^{-1} of XTT (2,3-bis-(2-methoxy-4-nitro-5-sulfophenyl)-2*H*-tetrazolium-5-carboxanilide) and incubated for three hours. The XTT enzymatic reduction was measured by reading the absorbance at 490 nm, with a reference wavelength of 630 nm. This procedure was repeated four times for each concentration.

HeLa cells expressing RFP labeled PCNA. HeLa cells were plated on 24 well optical dishes (*Ibidi*, Munich, Germany) and transfected with a mammalian expression plasmid coding for mRFP-tagged PCNA[62] using polyethylenimine (PEI). Time lapse microscopy was performed on an UltraView spinning disc confocal microscopy system (*PerkinElmer*, UK) equipped with temperature, humidity and CO_2 incubation controller (*Olympus*) and a 63×/1.4 Plan-Fluor oil immersion lens (*Nikon*).

Microirradiation and confocal microscopy. COSS compound **4** was added at 20 μM concentration to the HeLa cells expressing RFP-labeled PCNA. After 30 min of incubation, a cell was first imaged and then irradiated at the micrometer spot within the nucleus for 1.2 s using a 405 nm laser. The same cell was imaged after 5 min using a laser excitation of 488 nm to detect the fluorescein-labeled peptide and 561 nm to detect the RFP labeled PCNA.

Acknowledgements

We thank Dr. Holm Frauendorf (Georg-August University, Göttingen) for the HR-MS measurements. We acknowledge the collaboration with Prof. Dr. Robert Stark (Center of Smart Interfaces, Technische Universität Darmstadt) with respect to AFM measurements in the frame of the LOEWE Soft Control consortium.

References

1 M. Mahmood, D. Casciano, Y. Xu and A. S. Biris, *J. Appl. Toxicol.*, 2011, **32**, 10–19.
2 K. Ariga, Q. M. Ji, M. J. McShane, Y. M. Lvov, A. Vinu and J. P. Hill, *Chem. Mater.*, 2012, **24**, 728–737.
3 M. R. Longmire, M. Ogawa, P. L. Choyke and H. Kobayashi, *Bioconjugate Chem.*, 2011, **22**, 993–1000.
4 J. Fang, H. Nakamura and H. Maeda, *Adv. Drug Delivery Rev.*, 2011, **63**, 136–151.
5 V. Torchilin, *Adv. Drug Delivery Rev.*, 2011, **63**, 131–135.
6 F. Danhier, O. Feron and V. Preat, *J. Controlled Release*, 2010, **148**, 135–146.
7 M. Das, C. Mohanty and S. K. Sahoo, *Expert Opin. Drug Delivery*, 2009, **6**, 285–304.
8 A. E. Nel, L. Madler, D. Velegol, T. Xia, E. M. Hoek, P. Somasundaran, F. Klaessig, V. Castranova and M. Thompson, *Nat. Mater.*, 2009, **8**, 543–557.
9 A. Verma and F. Stellacci, *Small*, 2010, **6**, 12–21.
10 D. Napierska, L. C. Thomassen, D. Lison, J. A. Martens and P. H. Hoet, *Part. Fibre Toxicol.*, 2010, **7**, 39.
11 T. Yu, K. Greish, L. D. McGill, A. Ray and H. Ghandehari, *ACS Nano*, 2012, **6**, 2289–2301.
12 J. E. Fuller, G. T. Zugates, L. S. Ferreira, H. S. Ow, N. N. Nguyen, U. B. Wiesner and R. S. Langer, *Biomaterials*, 2008, **29**, 1526–1532.
13 S. W. Bae, W. Tan and J. I. Hong, *Chem. Commun.*, 2012, **48**, 2270–2282.
14 V. Lebret, L. Raehm, J. O. Durand, M. Smaihi, C. Gerardin, N. Nerambourg, M. H. V. Werts and M. Blanchard-Desce, *Chem. Mater.*, 2008, **20**, 2174–2183.
15 M. Green and P. M. Loewenstein, *Cell*, 1988, **55**, 1179–1188.
16 S. Santra, H. Yang, D. Dutta, J. T. Stanley, P. H. Holloway, W. Tan, B. M. Moudgil and R. A. Mericle, *Chem. Commun.*, 2004, 2810–2811.
17 L. Pan, Q. He, J. Liu, Y. Chen, M. Ma, L. Zhang and J. Shi, *J. Am. Chem. Soc.*, 2012, **134**, 5722–5725.
18 S. Angelos, Y. W. Yang, K. Patel, J. F. Stoddart and J. I. Zink, *Angew. Chem., Int. Ed.*, 2008, **47**, 2222–2226.
19 B. Trastoy, D. A. Bonsor, M. E. Perez-Ojeda, M. L. Jimeno, A. Mendez-Ardoy, J. M. G. Fernandez, E. J. Sundberg and J. L. Chiara, *Adv. Funct. Mater.*, 2012, **22**, 3191–3201.
20 Y. W. Yang, *Med. Chem. Commun.*, 2011, **2**, 1033–1049.
21 D. B. Cordes, P. D. Lickiss and F. Rataboul, *Chem. Rev.*, 2010, **110**, 2081–2173.
22 S. Fabritz, S. Hörner, D. Könning, M. Empting, M. Reinwarth, C. Dietz, B. Glotzbach, H. Frauendorf, H. Kolmar and O. Avrutina, *Org. Biomol. Chem.*, 2012, **10**, 6287–6293.
23 S. Fabritz, D. Heyl, V. Bagutski, M. Empting, E. Rikowski, H. Frauendorf, I. Balog, W. D. Fessner, J. J. Schneider, O. Avrutina and H. Kolmar, *Org. Biomol. Chem.*, 2010, **8**, 2212–2218.
24 Y. C. Lin and S. W. Kuo, *Polym. Chem.*, 2012, **3**, 162–171.
25 B. Trastoy, M. E. Perez-Ojeda, R. Sastre and J. L. Chiara, *Chem.–Eur. J.*, 2010, **16**, 3833–3841.
26 M. Lo Conte, S. Staderini, A. Chambery, N. Berthet, P. Dumy, O. Renaudet, A. Marra and A. Dondoni, *Org. Biomol. Chem.*, 2012, **10**, 3269–3277.
27 U. Dittmar, B. J. Hendan, U. Florke and H. C. Marsmann, *J. Organomet. Chem.*, 1995, **489**, 185–194.
28 F. J. Feher, K. D. Wyndham, M. A. Scialdone and Y. Hamuro, *Chem. Commun.*, 1998, 1469–1470.

29 D. Heyl, E. Rikowski, R. C. Hoffmann, J. J. Schneider and W. D. Fessner, *Chem.–Eur. J.*, 2010, **16**, 5544–5548.
30 J. Henig, E. Toth, J. Engelmann, S. Gottschalk and H. A. Mayer, *Inorg. Chem.*, 2010, **49**, 6124–6138.
31 T. L. Kaneshiro, X. Wang and Z. R. Lu, *Mol. Pharmaceutics*, 2007, **4**, 759–768.
32 X. J. Loh, Z. X. Zhang, K. Y. Mya, Y. L. Wu, C. B. He and J. Li, *J. Mater. Chem.*, 2010, **20**, 10634–10642.
33 D. Ding, K. Y. Pu, K. Li and B. Liu, *Chem. Commun.*, 2011, **47**, 9837–9839.
34 F. Olivero, F. Reno, F. Carniato, M. Rizzi, M. Cannas and L. Marchese, *Dalton Trans.*, 2012, **41**, 7467–7473.
35 C. McCusker, J. B. Carroll and V. M. Rotello, *Chem. Commun.*, 2005, 996–998.
36 Y. Gluzman, *Cell*, 1981, **23**, 175–182.
37 W. F. Scherer, J. T. Syverton and G. O. Gey, *J. Exp. Med.*, 1953, **97**, 695–710.
38 D. I. Zheleva, N. Z. Zhelev, P. M. Fischer, S. V. Duff, E. Warbrick, D. G. Blake and D. P. Lane, *Biochemistry*, 2000, **39**, 7388–7397.
39 T. Paunesku, S. Mittal, M. Protic, J. Oryhon, S. V. Korolev, A. Joachimiak and G. E. Woloschak, *Int. J. Radiat. Biol.*, 2001, **77**, 1007–1021.
40 S. M. Görisch and M. C. Cardoso, in *Proliferating Cell Nuclear Antigen*, ed. H. Lee and M. Szyf, Research SignPost, 2006, pp. 51–70.
41 L. H. Malkas, B. S. Herbert, W. Abdel-Aziz, L. E. Dobrolecki, Y. Liu, B. Agarwal, D. Hoelz, S. Badve, L. Schnaper, R. J. Arnold, Y. Mechref, M. V. Novotny, P. Loehrer, R. J. Goulet and R. J. Hickey, *Proc. Natl. Acad. Sci. U. S. A.*, 2006, **103**, 19472–19477.
42 J. Cmielova and M. Rezacova, *J. Cell. Biochem.*, 2011, **112**, 3502–3506.
43 J. M. Gulbis, Z. Kelman, J. Hurwitz, M. O'Donnell and J. Kuriyan, *Cell*, 1996, **87**, 297–306.
44 D. Yaffe and O. Saxel, *Nature*, 1977, **270**, 725–727.
45 G. Tunnemann, R. M. Martin, S. Haupt, C. Patsch, F. Edenhofer and M. C. Cardoso, *FASEB J.*, 2006, **20**, 1775–1784.
46 E. Oh, J. B. Delehanty, K. E. Sapsford, K. Susumu, R. Goswami, J. B. Blanco-Canosa, P. E. Dawson, J. Granek, M. Shoff, Q. Zhang, P. L. Goering, A. Huston and I. L. Medintz, *ACS Nano*, 2011, **5**, 6434–6448.
47 W. Yang, J. Gelles and S. M. Musser, *Proc. Natl. Acad. Sci. U. S. A.*, 2004, **101**, 12887–12892.
48 J. E. Hinshaw, B. O. Carragher and R. A. Milligan, *Cell*, 1992, **69**, 1133–1141.
49 J. M. de la Fuente and C. C. Berry, *Bioconjugate Chem.*, 2005, **16**, 1176–1180.
50 F. C. Jensen, H. Koprowski, A. J. Girardi and R. V. Gilden, *Proc. Natl. Acad. Sci. U. S. A.*, 1964, **52**, 53–59.
51 W. F. Scherer, J. T. Syverton and G. O. Gey, *J. Exp. Med.*, 1953, **97**, 695–710.
52 G. Saito, J. A. Swanson and K. D. Lee, *Adv. Drug Delivery Rev.*, 2003, **55**, 199–215.
53 *Handbook of Biological Confocal Microscopy*, Springer Science + Business Media, LLC, James B. Pawley, 3rd edn, 2006.
54 T. R. Rodriguez and R. Garcia, *Appl. Phys. Lett.*, 2004, **84**, 449–451.
55 C. Dietz, E. T. Herruzo, J. R. Lozano and R. Garcia, *Nanotechnology*, 2011, **22**, 125708.
56 R. Garcia and E. T. Herruzo, *Nat. Nanotechnol.*, 2012, **7**, 217–226.
57 G. Tunnemann, G. Ter-Avetisyan, R. M. Martin, M. Stockl, A. Herrmann and M. C. Cardoso, *J. Pept. Sci.*, 2008, **14**, 469–476.
58 W. A. Zhang, J. Y. Yuan, S. Weiss, X. D. Ye, C. L. Li and A. H. E. Muller, *Macromolecules*, 2011, **44**, 6891–6898.
59 X. Zhang, E. R. Chan and S. C. Glotzer, *J. Chem. Phys.*, 2005, **123**, 184718.
60 Y. C. Lin and S. W. Kuo, *J. Polym. Sci., Part A: Polym. Chem.*, 2011, **49**, 2127–2137.
61 H. J. Ryser, *Nature*, 1967, **215**, 934–936.
62 A. Sporbert, P. Domaing, H. Leonhardt and M. C. Cardoso, *Nucleic Acids Res.*, 2005, **33**, 3521–3528.
63 P. Perucca, O. Cazzalini, O. Mortusewicz, D. Necchi, M. Savio, T. Nardo, L. A. Stivala, H. Leonhardt, M. C. Cardoso and E. Prosperi, *J. Cell Sci.*, 2006, **119**, 1517–1527.
64 M. Hallbrink, A. Floren, A. Elmquist, M. Pooga, T. Bartfai and U. Langel, *Biochim. Biophys. Acta Biomembranes*, 2001, **1515**, 101–109.
65 E. Rikowski and H. C. Marsmann, *Polyhedron*, 1997, **16**, 3357–3361.
66 F. J. Feher, K. D. Wyndham, D. Soulivong and F. Nguyen, *J. Chem. Soc., Dalton Trans.*, 1999, 1491–1497.
67 D. A. Scudiero, R. H. Shoemaker, K. D. Paull, A. Monks, S. Tierney, T. H. Nofziger, M. J. Currens, D. Seniff and M. R. Boyd, *Cancer Res.*, 1988, **48**, 4827–4833.
68 P. R. Leroueil, S. Hong, A. Mecke, J. R. Baker Jr., B. G. Orr and M. M. Banaszak Holl, *Acc. Chem. Res.*, 2007, **40**, 335–342.
69 P. R. Leroueil, S. A. Berry, K. Duthie, G. Han, V. M. Rotello, D. Q. McNerny, J. R. Baker Jr., B. G. Orr and M. M. Holl, *Nano Lett.*, 2008, **8**, 420–424.
70 F. J. Feher and K. D. Wyndham, *Chem. Commun.*, 1998, 323–324.

Supplemental Information

Cube-octameric silsesquioxane-mediated cargo peptide delivery into living cancer cells

Sebastian Hörner, Sebastian Fabritz, Henry D. Herce, Olga Avrutina, Christian Dietz, Robert W. Stark, M. Cristina Cardoso, and Harald Kolmar

Content

Compound 2 (Fmoc-L-cysteine heptaamino-COSS) and 2a (Fmoc-(S-trityl)-L-cysteine heptaamino-COSS)

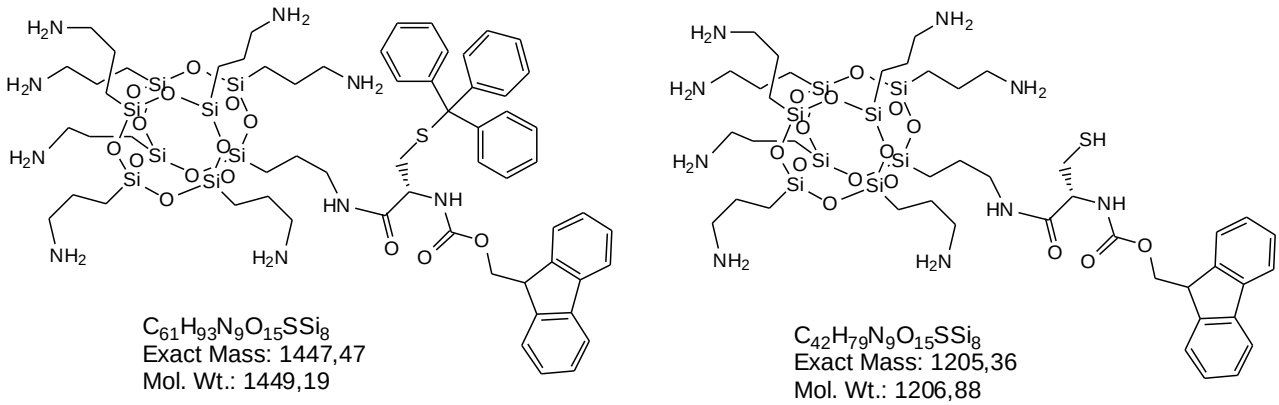

Fig. S1: Chemical structure of Fmoc-(S-trityl)-L-cysteine heptaamino-COSS **2a** (left) and unprotected Fmoc-L-cysteine heptaamino-COSS **2** (right).

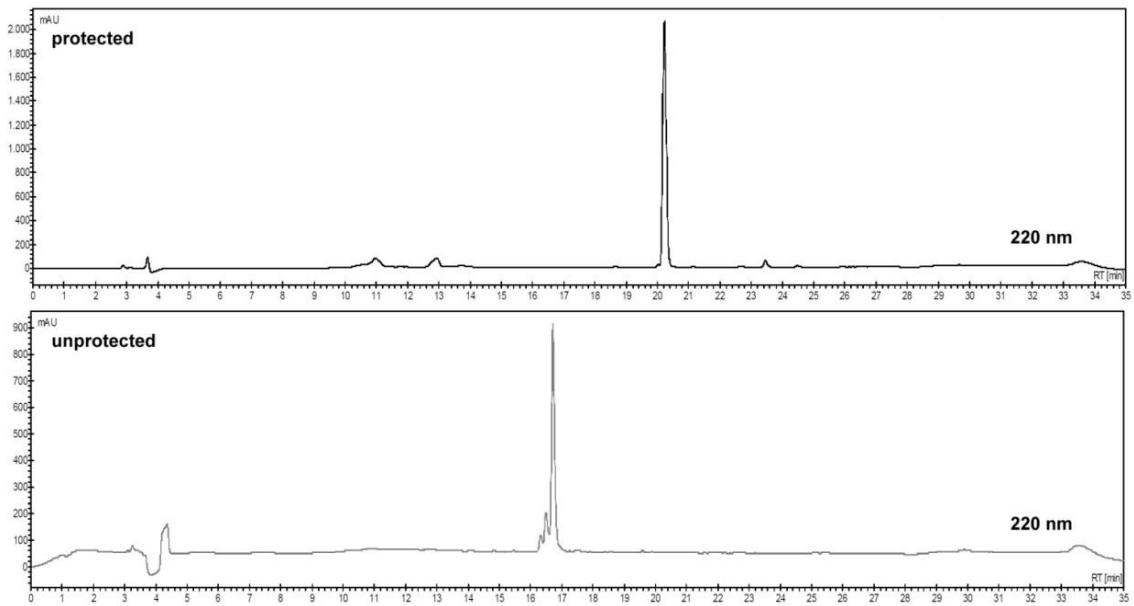

Fig. S2: Analytical RP-HPLC traces of trityl-protected (**2a**) and deprotected Fmoc-L-cysteine heptaamino-COSS **2**. (*Varian* 940-LC equipped with a *Phenomenex* Luna C_{18} column (5u, 100 A, 250×4.60 mm, 5 µm). Eluent A: 0.1% aq. trifluoroacetic acid (TFA), eluent B: 90 % aq. acetonitrile in 0.1% aq. TFA; 10 → 80% B in 20 min preceded by 5 min isocratic 10 % B at a flow rate of 1 mL min^{-1}).

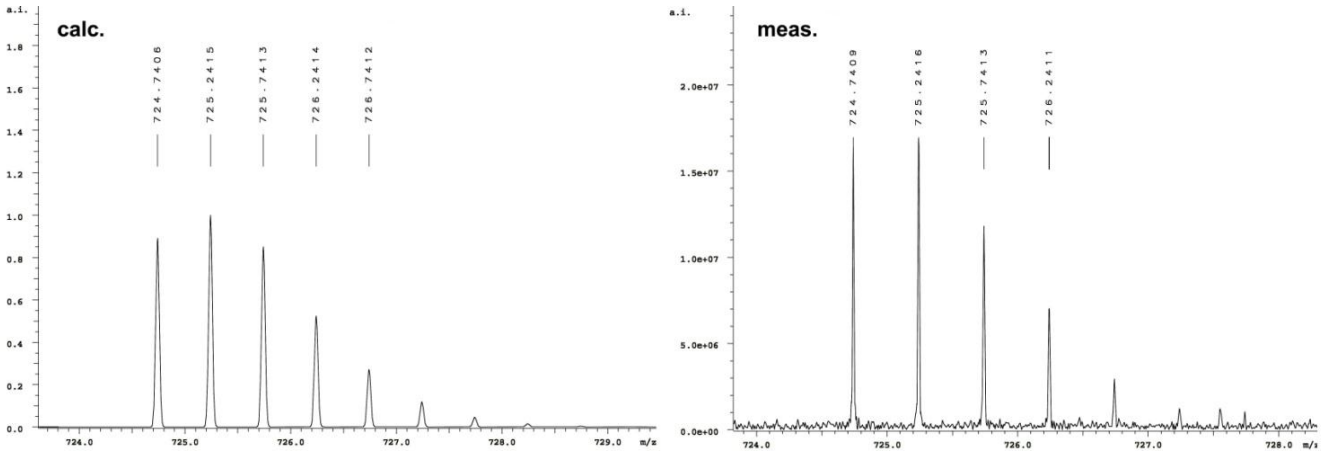

Fig. S3: HR-MS measurement of compound **2a**; left: calculated isotopic pattern $[M+2H]^{2+}$= 724.7406; right: measured isotopic pattern $[M+2H]^{2+}$= 724.7409.

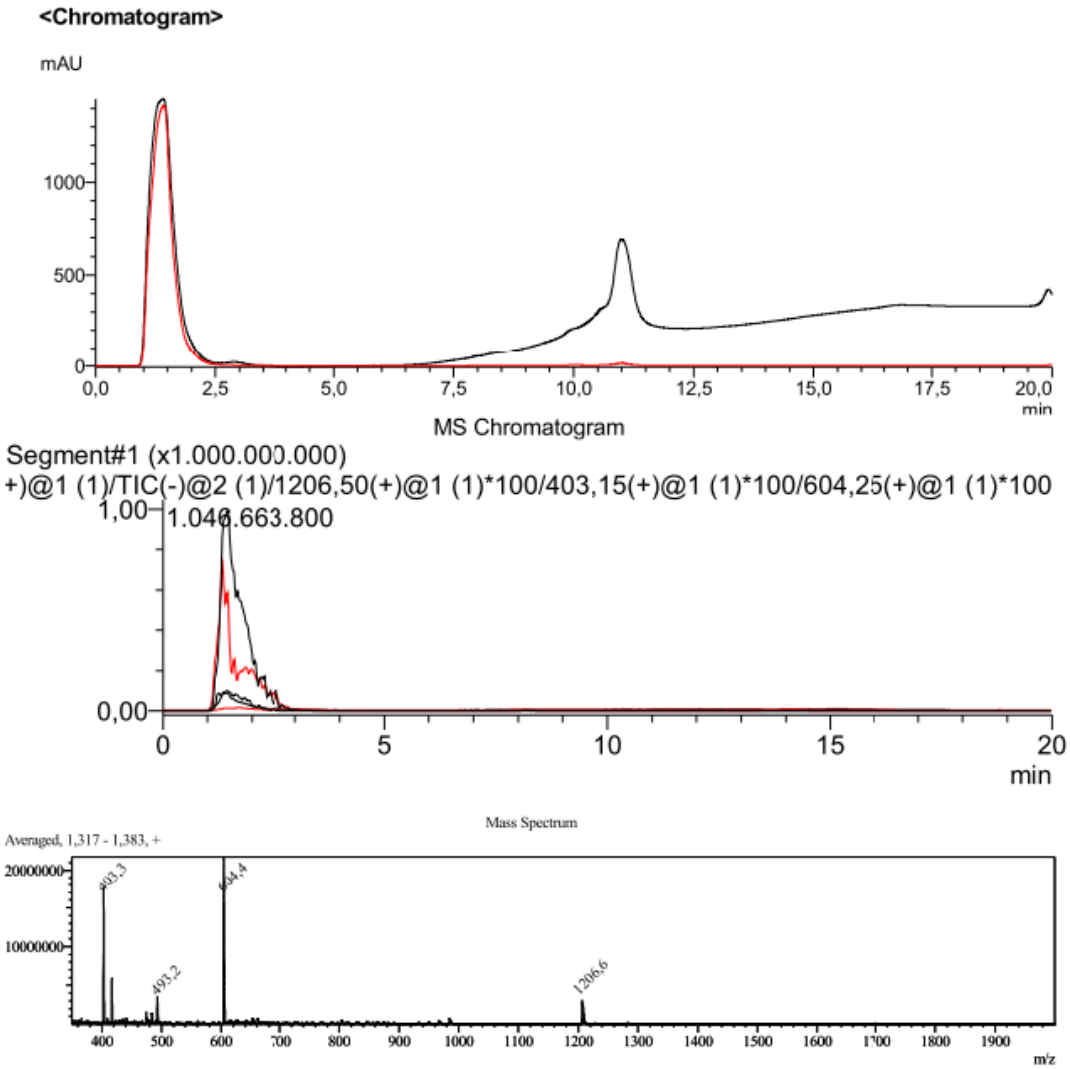

Fig. S4 LC-MS (ESI) measurement of compound **2**.

Compound 3 (fluorescein-labeled PCNA binding peptide)

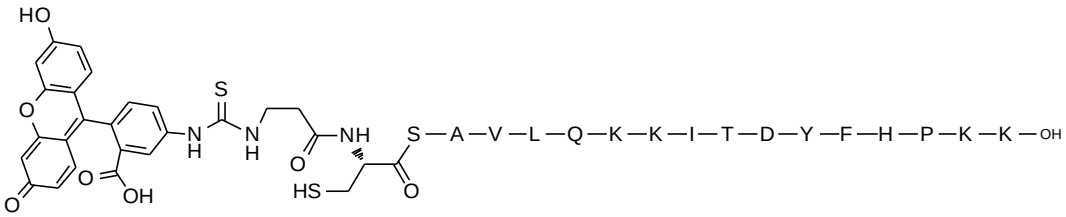

Chemical Formula: $C_{116}H_{164}N_{26}O_{30}S_2$
Exact Mass: 2465,15
Molecular Weight: 2466,83

Fig. S5: Amino acid sequence and chemical structure of fluorescein-labeled PCNA binding peptide **3**.

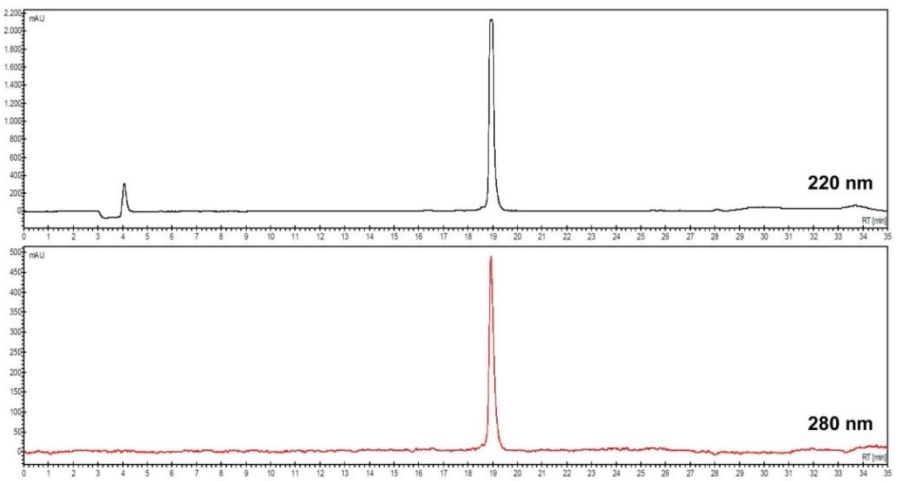

Fig. S6: Analytical RP-HPLC traces of FITC-labeled PCNA binding peptide **3** (*Varian* 940-LC equipped with a *Phenomenex* Luna C_{18} column (5u, 100 A, 250×4.60 mm, 5 µm). Eluent A: 0.1% aq. trifluoroacetic acid (TFA), eluent B: 90 % aq. acetonitrile in 0.1% aq. TFA; 25 → 50% B in 20 min preceded by 5 min isocratic 25 % B at a flow rate of 1 mL min^{-1}).

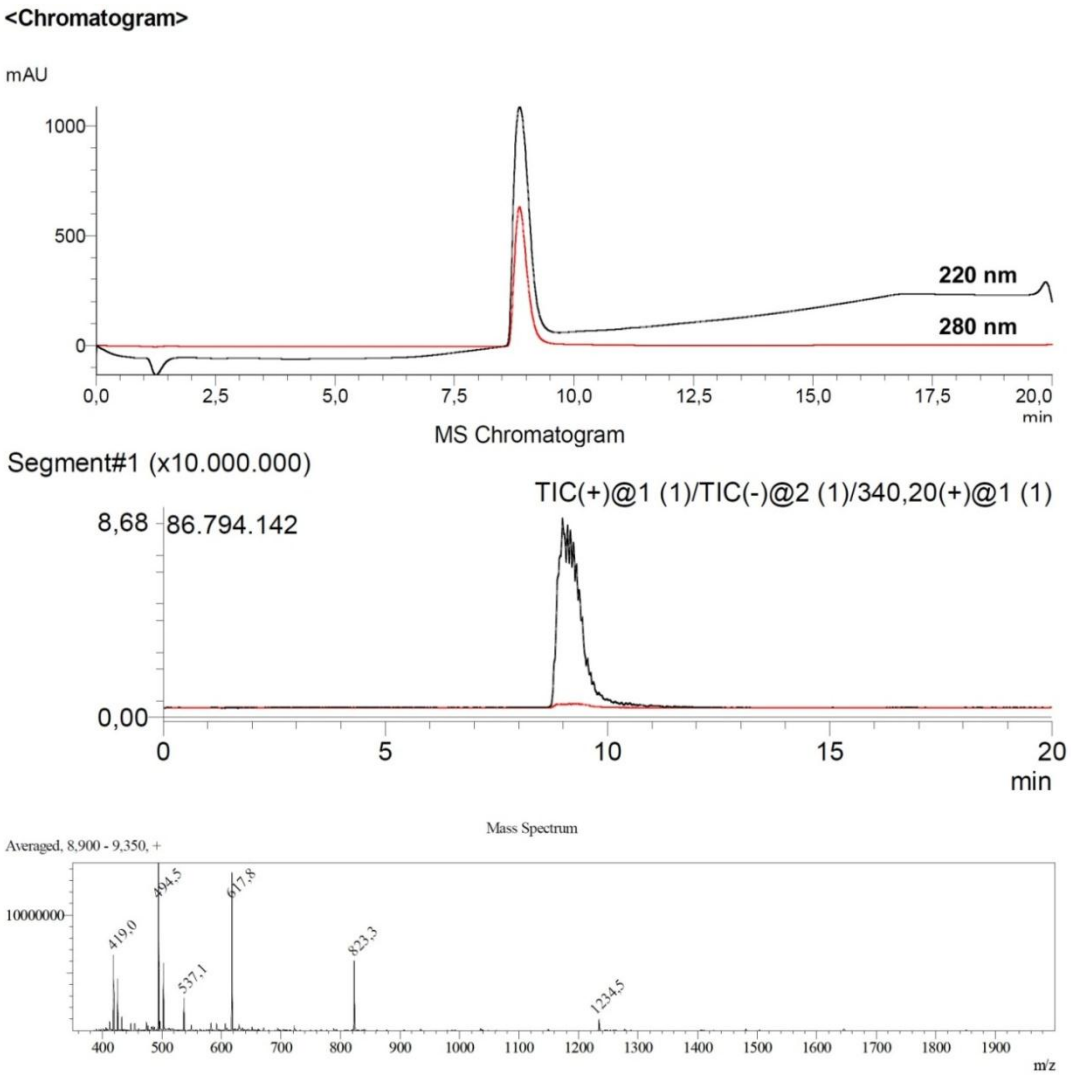

Fig. S7: LC-MS (ESI) measurement of the purified fluorescein-labeled PCNA binding peptide **3**.

Compound 4 (fluorescently labeled PCNA binding peptide coupled to Fmoc-L-cysteine heptaamino-COSS)

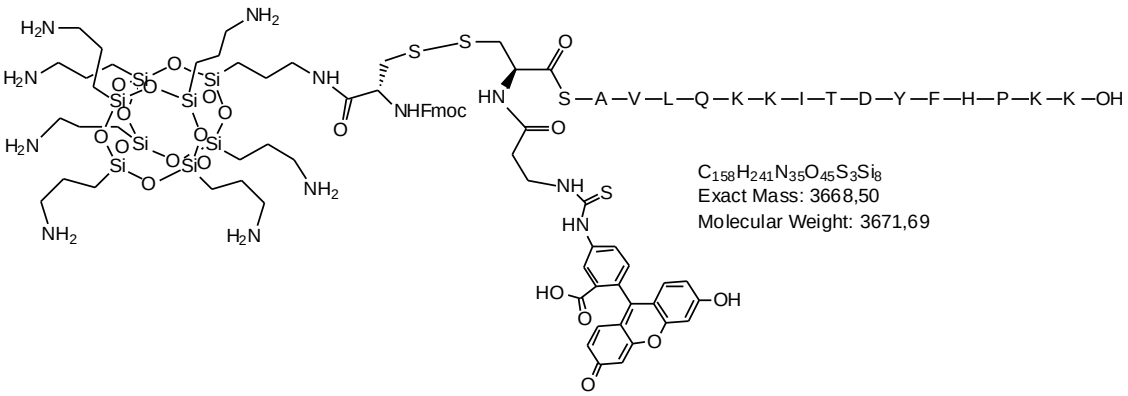

Fig. S8: Chemical structure of compound **4**.

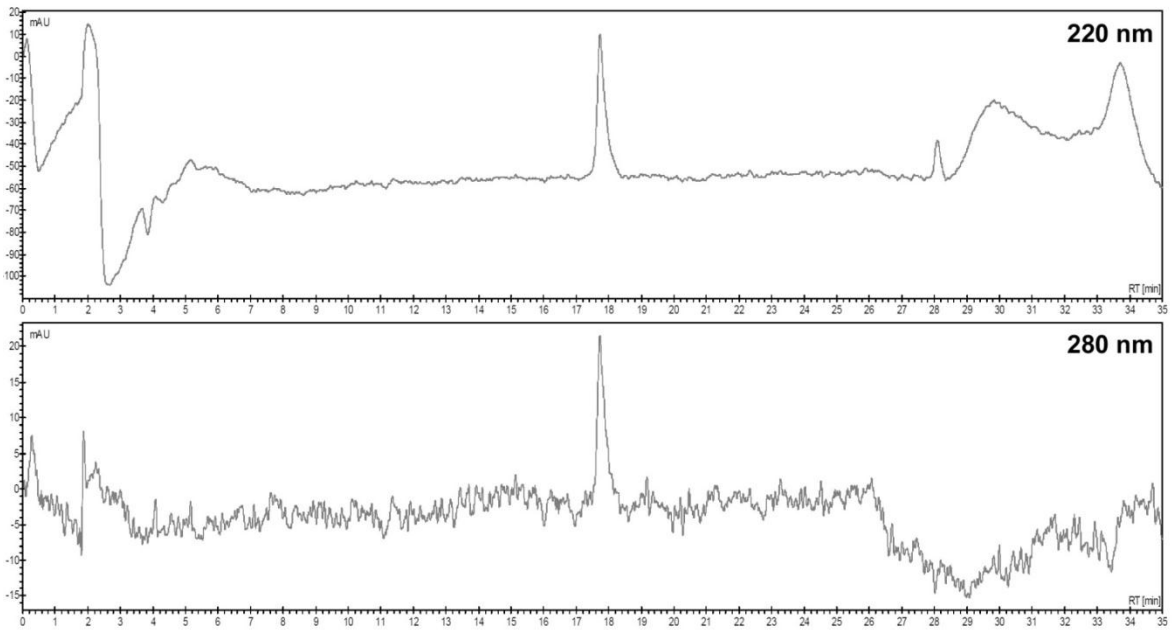

Fig. S9: Analytical RP-HPLC traces of compound **4** (*Varian* 940-LC equipped with a *Phenomenex* Luna C_{18} column (5u, 100 A, 250×4.60 mm, 5 µm). Eluent A: 0.1% aq. trifluoroacetic acid (TFA), eluent B: 90 % aq. acetonitrile in 0.1% aq. TFA; 25 → 50% B in 20 min preceded by 5 min isocratic 10 % B at a flow rate of 1 mL min^{-1}).

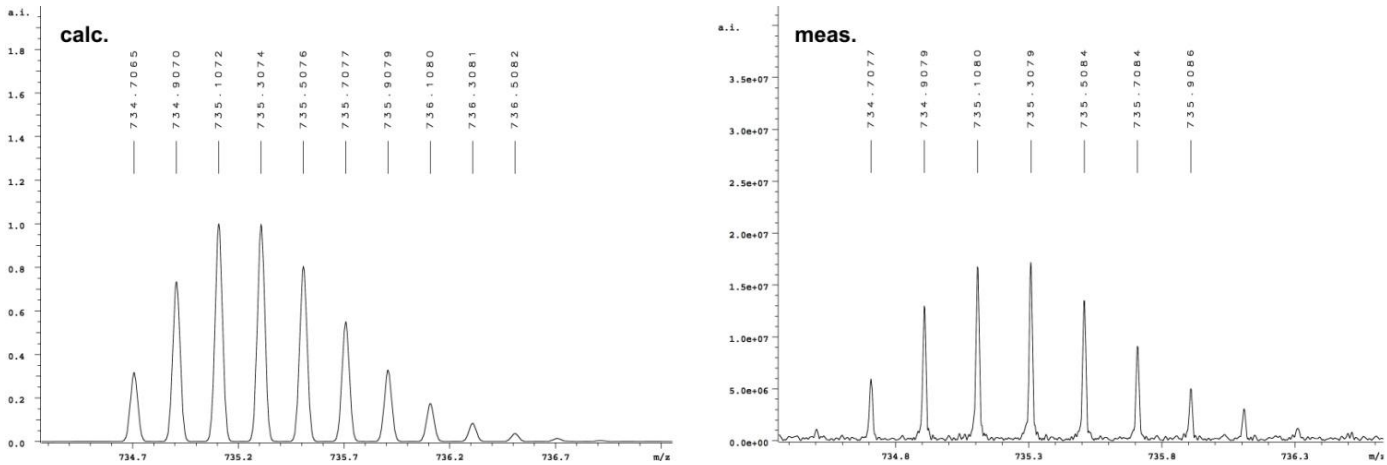

Fig. S10: HR-MS measurement of compound **4**; left: calculated isotopic pattern $[M+5H]^{5+}$= 734.7065; right: measured isotopic pattern $[M+5H]^{5+}$= 734.7077.

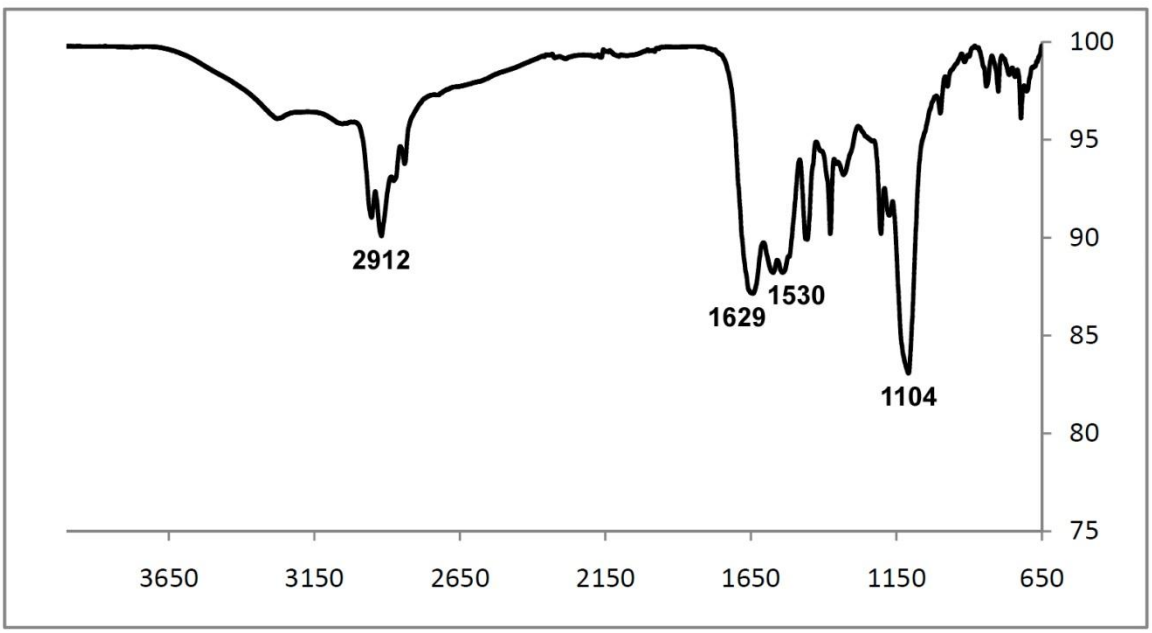

Fig. S11: FT-IR spectrum of compound **4**.

Compound 5 (cysteine-β-alanine-fluorescein hepataamino-COSS), 5a (cysteine-(S-trityl)-β-alanine-fluorescein), and 5b (cysteine-(S-trityl)-β-alanine-fluorescein hepataamino-COSS)

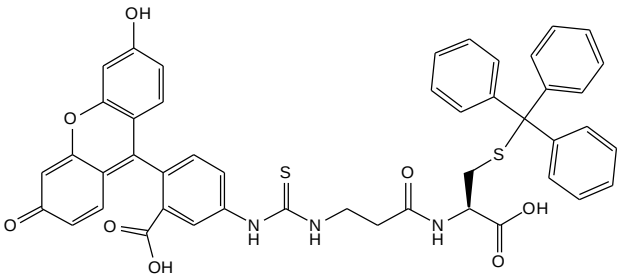

$C_{46}H_{37}N_3O_8S_2$
Exact Mass: 823,2
Mol. Wt.: 823,93

Fig. S12: Chemical structure of compound **5a**.

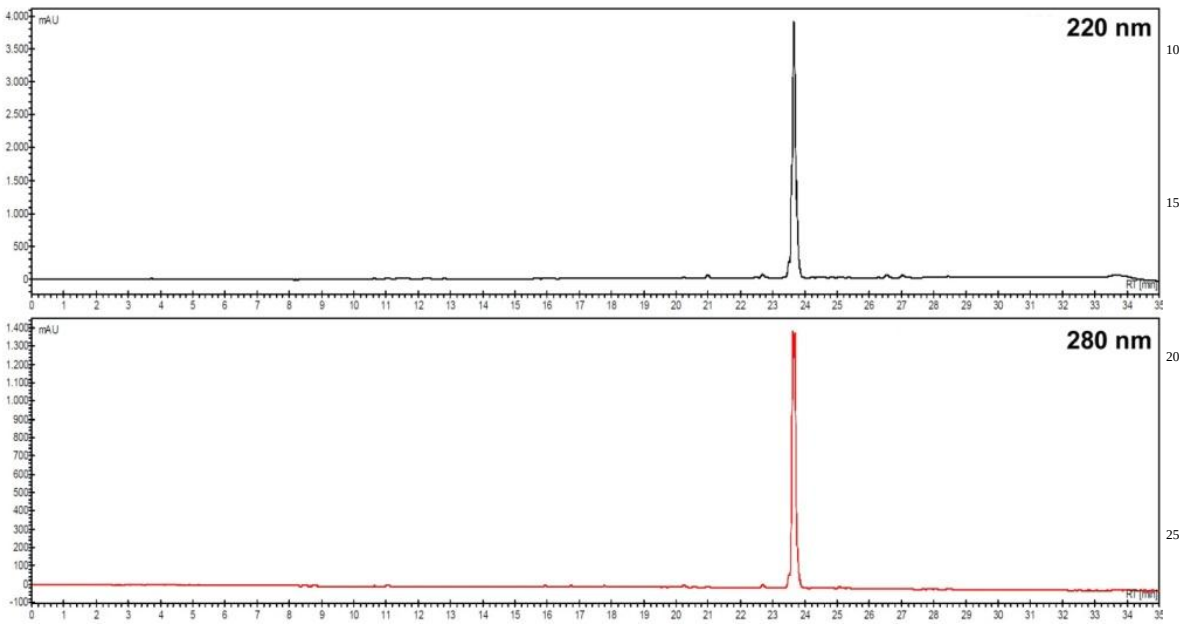

Fig. S13: Analytical RP-HPLC traces of compound **5a**. (*Varian* 940-LC equipped with a *Phenomenex* Luna C_{18} column (5u, 100 A, 250×4.60 mm, 5 µm). Eluent A: 0.1% aq. trifluoroacetic acid (TFA), eluent B: 90 % aq. acetonitrile in 0.1% aq. TFA; 10 → 100% B in 20 min preceded by 5 min isocratic 10 % B at a flow rate of 1 mL min^{-1}).

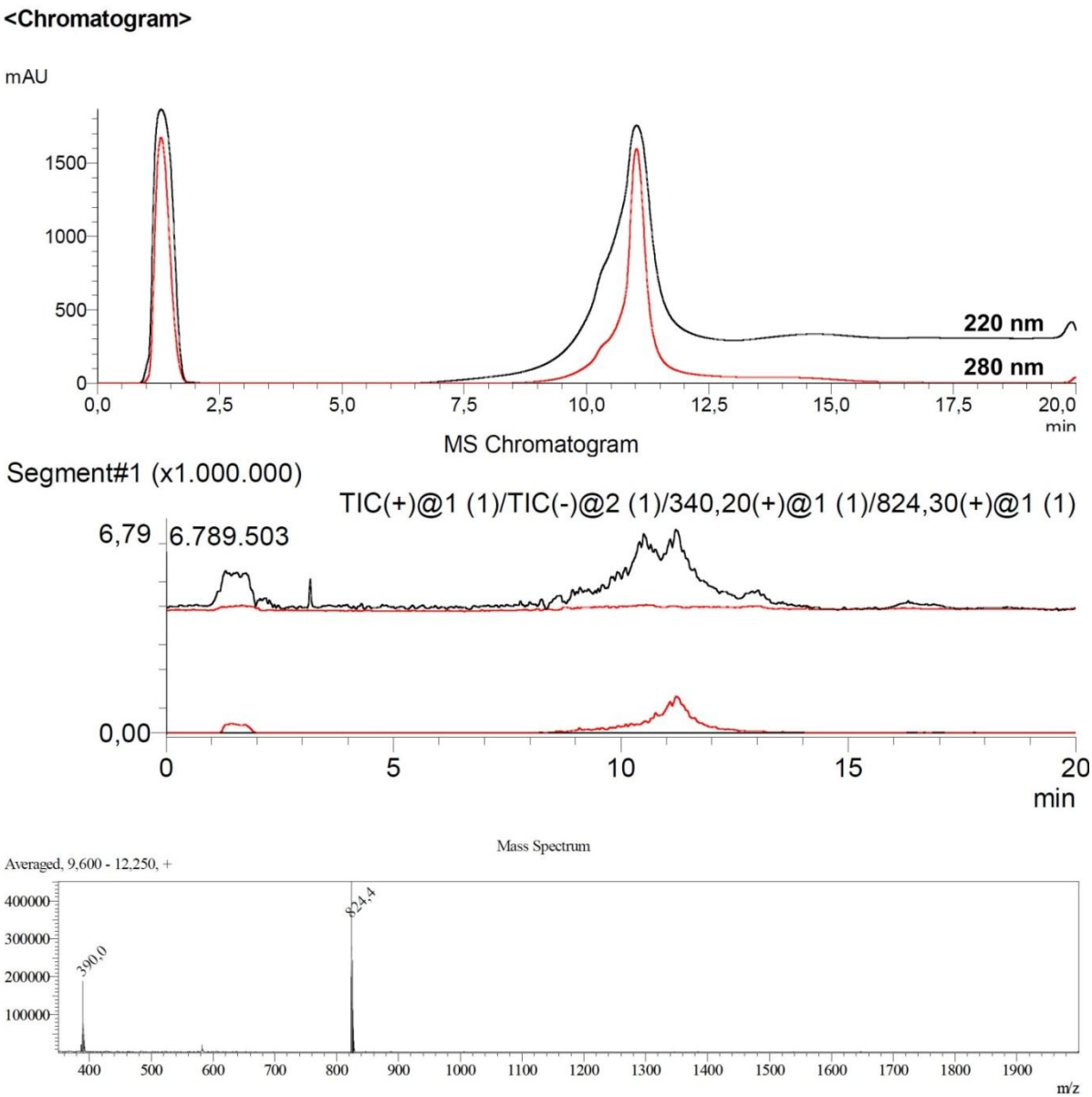

Fig. S14: LC-MS (ESI) measurement of compound **5a**.

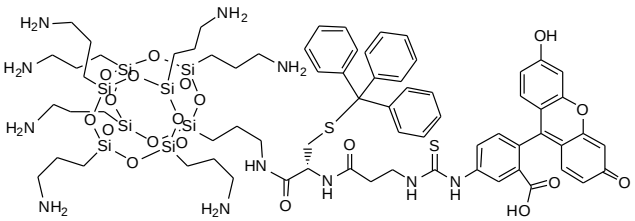

$C_{70}H_{99}N_{11}O_{19}S_2Si_8$
Exact Mass: 1685,47
Molecular Weight: 1687,41

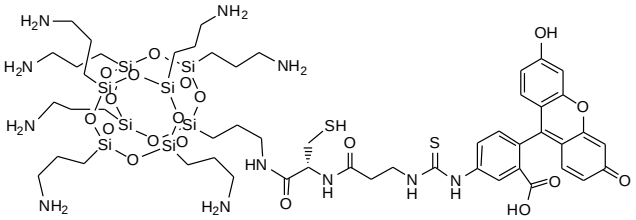

$C_{51}H_{85}N_{11}O_{19}S_2Si_8$
Exact Mass: 1443,36
Molecular Weight: 1445,10

Fig. S15: Chemical structures of trityl protected **5b** (left) and unprotected cysteine-β-alanine-fluorescein hepataamino-COSS **5** (right).

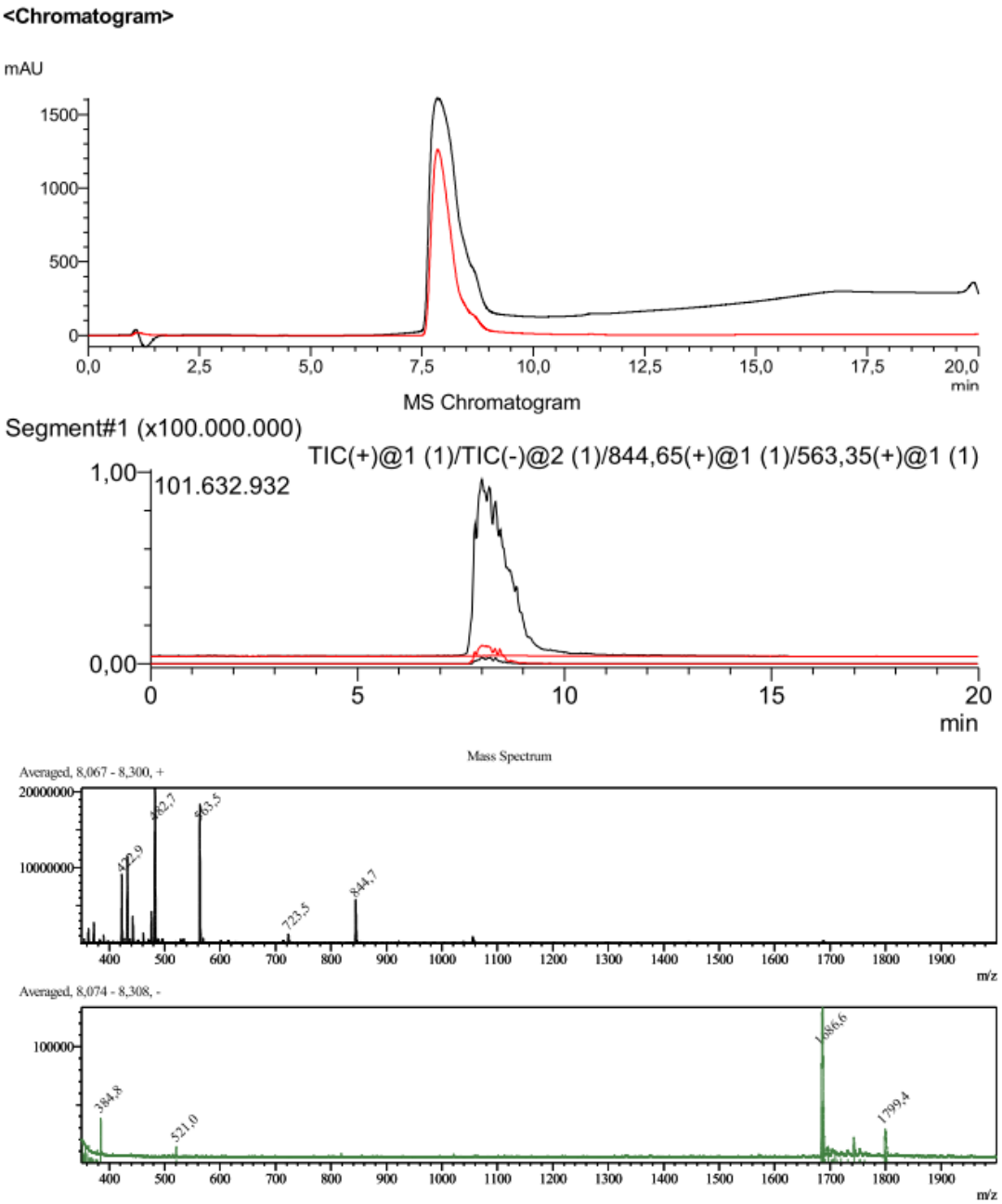

Fig. S16: LC-MS (ESI) measurement of cysteine-(S-trityl)-β-alanine-fluorescein hepataamino-COSS **5b**.

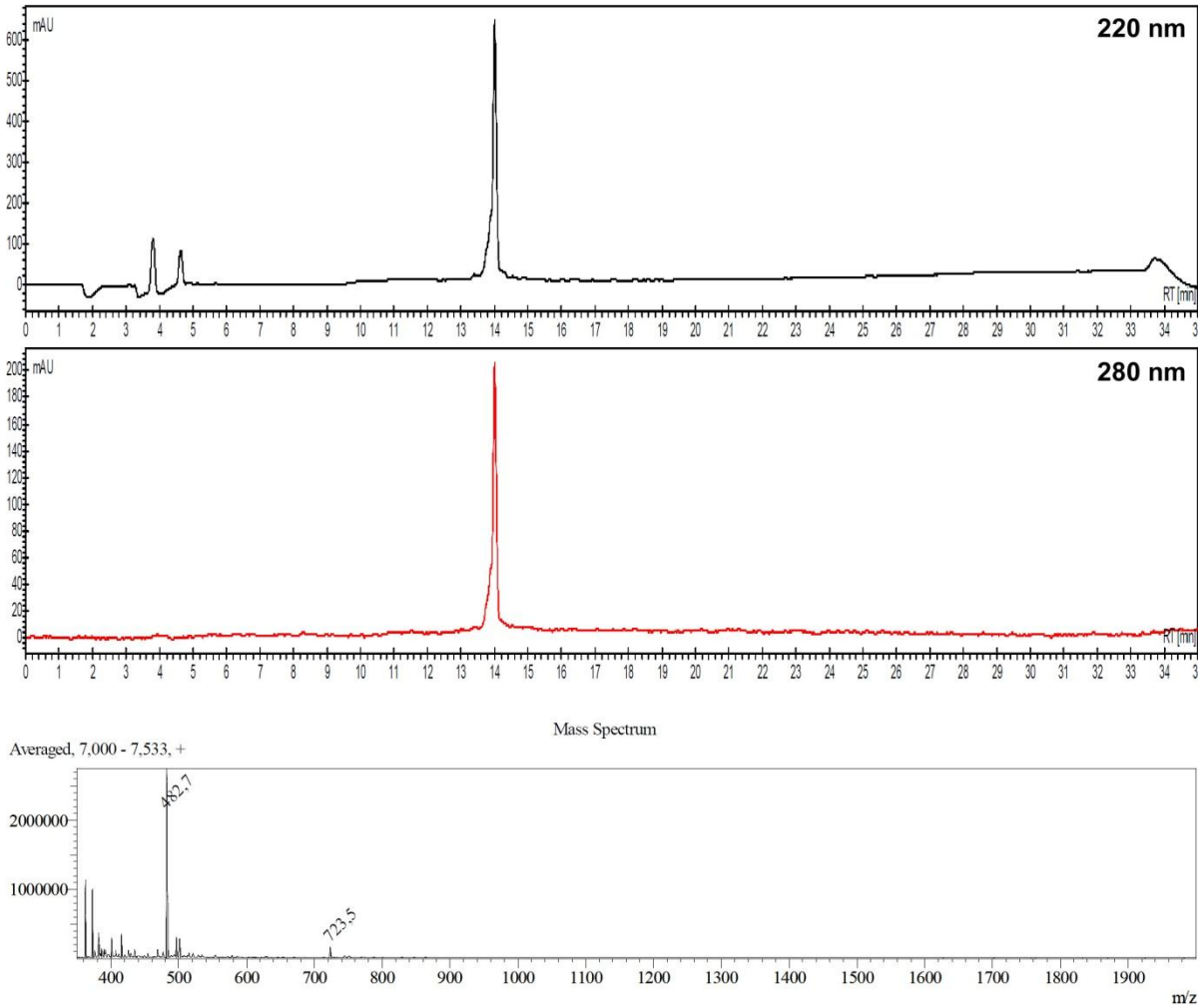

Fig. S17: Analytical RP-HPLC traces (*Varian* 940-LC equipped with a *Phenomenex* Luna C_{18} column (5u, 100 A, 250×4.60 mm, 5 µm). Eluent A: 0.1% aq. trifluoroacetic acid (TFA), eluent B: 90 % aq. acetonitrile in 0.1% aq. TFA; 10 → 100% B in 20 min preceded by 5 min isocratic 10 % B at a flow rate of 1 mL min^{-1}) and MS analysis of cysteine-β-alanine-fluorescein hepataamino-COSS **5**.

Microirradiation experiment and subsequent co-localization of fluorescently labeled PCNA binding peptide and RFP labeled PCNA after the addition of compound 4

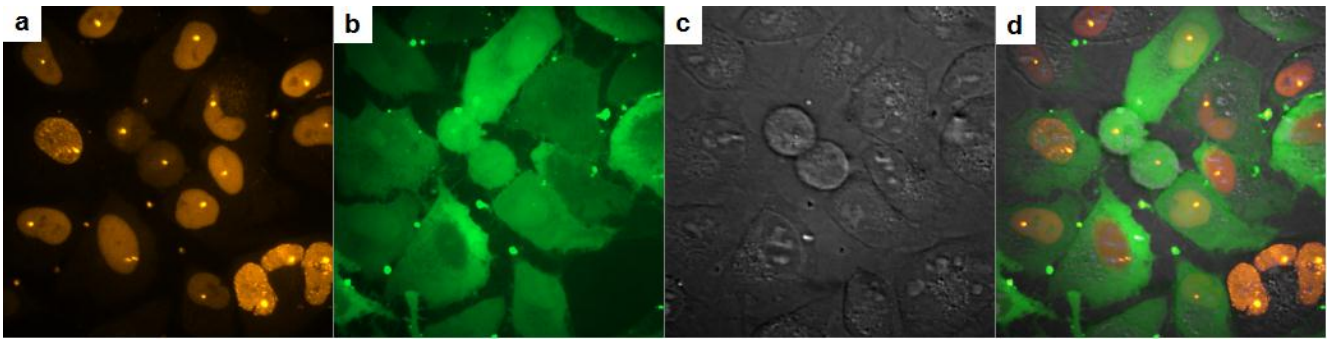

Fig. S18: Fluorescence microscopic analysis of irradiated HeLa cells 30 minutes after the addition of compound **4**. (a) PCNA (red); (b) cleaved fluorescein-labeled peptide **3** (green); (c) contrast image ; (d) overlay.